Physics in Medicine & Biology

PAPER

Improved single photon time resolution for analog SiPMs with front end readout that reduces influence of electronic noise

To cite this article: Joshua W Cates *et al* 2018 *Phys. Med. Biol.* **63** 185022

IOP Publishing Phys. Med. Biol. 63 (2018) 185022 (11pp) https://doi.org/10.1088/1361-6560/aadbcd

Physics in Medicine & Biology

IPEM Institute of Physics and Engineering in Medicine

PAPER

Improved single photon time resolution for analog SiPMs with front end readout that reduces influence of electronic noise

Joshua W Cates[1], Stefan Gundacker[2,3], Etiennette Auffray[2], Paul Lecoq[2] and Craig S Levin[1,4,5,6,7]

[1] Department of Radiology, Stanford University, Stanford, CA, United States of America
[2] European Organization for Nuclear Research (CERN), Geneva, Switzerland
[3] Universitá degli Studi di Milano-Bicocca, Milano, Italy
[4] Department of Bioengineering, Stanford University, Stanford, CA, United States of America
[5] Department of Physics, Stanford University, Stanford, CA, United States of America
[6] Department of Electrical Engineering, Stanford University, Stanford, CA, United States of America
[7] Author to whom any correspondence should be addressed.

E-mail: cslevin@stanford.edu

Keywords: silicon photomultiplier, single photon time resolution, timing resolution

RECEIVED
10 January 2018

REVISED
13 August 2018

ACCEPTED FOR PUBLICATION
21 August 2018

PUBLISHED
19 September 2018

Abstract

A key step to improve the coincidence time resolution of positron emission tomography detectors that exploit small populations of promptly emitted photons is improving the single photon time resolution (SPTR) of silicon photomultipliers (SiPMs). The influence of electronic noise has previously been identified as the dominant factor affecting SPTR for large area, analog SiPMs. In this work, we measure the achievable SPTR with front end electronic readout that minimizes the influence of electronic noise. With this readout circuit, the SPTR measured for one FBK NUV single avalanche photodiode (SPAD) was also achieved with a $1 \times 1\,mm^2$ FBK NUV SiPM. SPTR for large area devices was also significantly improved. The measured SPTRs for $3 \times 3\,mm^2$ Hamamatsu and SensL SiPMs were $\leqslant$150 ps FWHM, and SPTR $\leqslant$100 ps FWHM was measured for $3 \times 3\,mm^2$ and $4 \times 4\,mm^2$ FBK NUV and NUV-HD SiPMs. We also explore additional factors affecting the achievable SPTR for large area, analog SiPMs when the contribution of electronic noise is minimized and pinpoint potential areas of improvement to further reduce the SPTR of large area sensors towards that achievable for a single SPAD.

1. Introduction and motivation

With increasing efforts to improve the timing performance of scintillation detectors for time-of-flight positron emission tomography (TOF-PET), sub-100 ps coincidence time resolution (CTR) is achievable with lutetium-based inorganic scintillators (Nemallapudi *et al* 2015, Cates and Levin 2016, Gundacker *et al* 2016a) using state-of-the-art silicon photomultipliers (SiPMs) (Piemonte *et al* 2016, Otte *et al* 2017, SensL 2017) and optimized signal processing techniques (Seifert *et al* 2009, Schaart *et al* 2010, Gola *et al* 2011, 2012). Future efforts aim to improve CTR towards 10 ps full-width-at-half-maximum (FWHM) (Lecoq 2017), where the accuracy of 511 keV photon localization along system lines of response approaches the intrinsic spatial resolution of a clinical system, as dictated by positron range, annihilation photon acolinearity, and detector element size (Levin and Hoffman 1999). With this in mind, it is of interest to also begin exploring methods to improve the single photon time resolution (SPTR) of analog silicon photomultipliers (SiPMs). For relatively fast and bright inorganic scintillation materials with luminescence kinetics similar to LSO:Ce, SPTR does not have a strong influence on CTR (Gundacker *et al* 2013). For that case, significant improvements in SPTR yield minor improvements in CTR. However, many researchers are now investigating improvements in CTR by exploiting small populations of prompt photons (Lecoq *et al* 2014, Gundacker *et al* 2016b, Kwon *et al* 2016a, Brunner and Schaart 2017). With such an approach, SPTR can have a stronger influence on CTR. Figure 1 shows the statistical limit on coincidence time resolution via the Cramér–Rao Lower Bound (CRLB) (Seifert *et al* 2012, Cates *et al* 2015) for 3 mm length LSO:Ce,Ca(0.4%) crystals as a function of SPTR and prompt photon yield in the crystal. Even for a case where

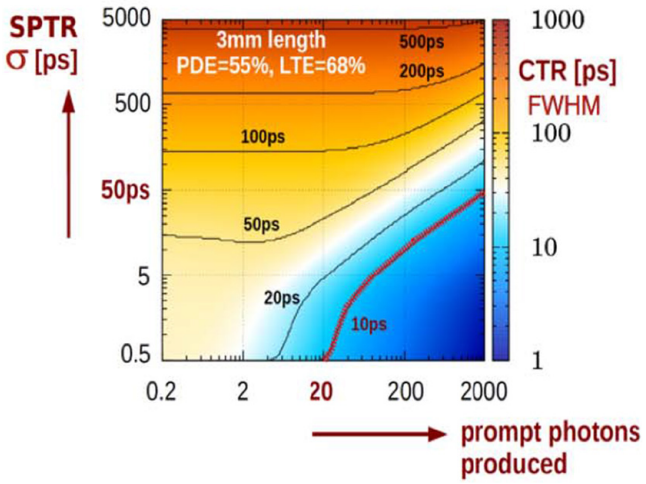

Figure 1. Cramér–Rao Lower Bound (CRLB) on coincidence time resolution for a 3 mm length LSO:Ce,Ca(0.4%) crystal where SPTR and the number of 'prompt' photons produced in the crystal are parametrically varied (Gundacker *et al* 2016b) around the measured values of 50 ps sigma (117.5 ps FWHM) for the best commercially available SiPMs and 20 Cherenkov prompt photons produced by the recoil electron in LSO crystals.

scintillation photon transit time jitter in the crystal is minimized (3 mm length) and many prompt photons are produced, CTR will not improve towards this 10 ps goal unless SPTR can also be significantly reduced.

Previous work by Fondazione Bruno Kessler (FBK) has investigated what factors contribute to SPTR for analog SiPMs, and concluded that timing jitter due to the influence of electronic noise is the dominant factor degrading SPTR for large area sensors (Acerbi *et al* 2014a, 2015a). Parasitic capacitance increases with device size, shaping the slope of the signal rise time and degrading signal-to-noise ratio (SNR). In addition, non-optimal bandwidth from front-end signal processing of SiPM pulses can elongate signal rise time, further increasing the influence of electronic noise on SPTR. Techniques to reduce the effective device capacitance have previously been used for readout of large area, direct-conversion silicon gamma detectors (Kwon *et al* 2015, 2016b). For these techniques, a unity gain amplifier connects the cathode and anode of the device. Signal from the cathode is passed to the anode, balancing the voltage across the device, which will also reduce the effective device capacitance. Another approach to achieve this reduction in effective device capacitance with passive components is outlined in Zhang and Schmand *et al* (2016). In that case, the two terminals of the device are connected by one side of a transformer, and further signal processing is isolated on the second side of the transformer. If these capacitance compensation techniques can be used in combination with fast, low noise front-end readout, they are potential methods to reduce the contribution of electronic noise on SPTR for large area SiPMs.

In this work, we implemented the passive capacitance compensation technique outlined in Zhang and Schmand *et al* (2016) into front end readout for analog SiPMs. With this readout technique, we estimated the contribution to timing jitter from electronic noise. We also measured achievable SPTR with various SiPMs, comparing the measured values with those reported with the NINO ASIC (Nemallapudi *et al* 2016). With these analyses, we further investigate other possible contributions to degraded SPTR when the timing jitter due to electronic noise is minimized.

2. Materials and experimental methods

2.1. Front-end readout and SiPMs

Some challenges with active capacitance compensation techniques (Kwon *et al* 2015, 2016b) can include difficulty to stabilize the circuit and injection of noise from the bootstrap amplifier. Moreover, adequate amplification from operational amplifiers typically leaves low bandwidth, increased signal rise time and reduced SNR of the single photon response shape from the SiPM. Attractive aspects of passive techniques to compensate for device capacitance include no injection of noise in the open connection between the two nodes of the device and no issues with circuit instability in the readout. Given these considerations, we created a circuit to test achievable SPTR with analog SiPMs using a passive compensation technique.

The passive compensation circuit is a modified version of that outlined in Zhang and Schmand *et al* (2016), where a balun transformer is connected between the cathode and anode of the SiPM in a balanced-to-unbalanced configuration to two Minicircuits MAR-6 RF amplifiers (Minicircuits 2017) in cascade. A simple schematic of the circuit is shown in figure 2(a), and an example of a printed board is shown in figure 2(b). The balun transformer used in the passive compensation circuit is a Macom MABA-007159 (MACOM 2018) (50 Ω impedance and 1:1 turn ratio). Also shown in figure 2(c) is the average of 700 single photon pulses from a 3 × 3 mm^2

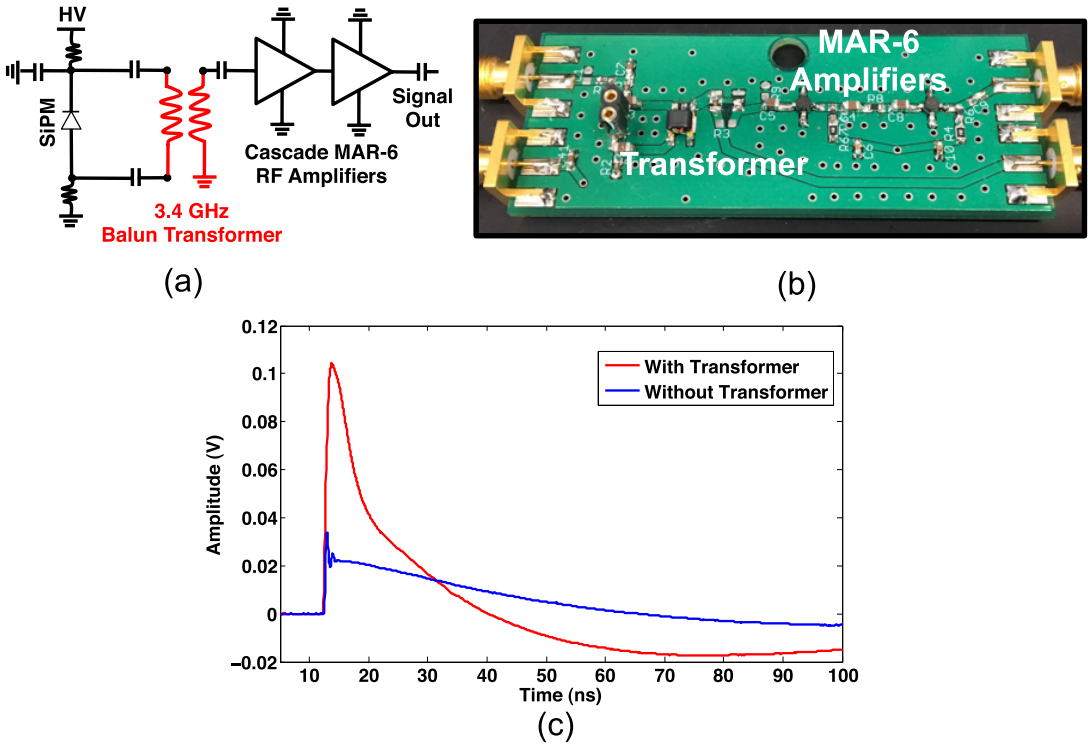

Figure 2. Schematic of the circuit with passive capacitance compensation is shown in (a), and an example of an assembled circuit is shown in (b). The average of 700 single photon pulses from a 3 × 3 mm^2 Hamamatsu S13360 SiPM biased at 58.5 V with and without the balun transformer in place is shown in (c).

Hamamatsu S13360 SiPM biased at 58.5 V using the example circuit in figure 2(b) with and without the balun transformer in place (offset in time for clarity). Identical circuits were used for the comparison without and with the transformer in figure 2(c). The only difference between them was the presence or absence of the transformer. One important note is that the balanced-to-unbalanced connection of the transformer to the SiPM should result in 2-fold increase in pulse amplitude. The observed factor of ∼3.5 improvement in single photon pulse amplitude shown in figure 2(c) suggests an additional boost from a lower effective terminal capacitance, as described in Zhang and Schmand *et al* (2016). This readout circuit will be referred to as the compensation circuit for the remainder of the manuscript.

2.2. SPTR measurements

SPTR was measured with the compensation circuit and compared with those already measured using the NINO ASIC (Nemallapudi *et al* 2016) for a variety of SiPMs shown in table 1. The experimental setups, shown in figure 3, consisted of a 420 nm wavelength laser with a timing jitter of 42 ps FWHM illuminating the SiPMs. For the measurements with the NINO ASIC, the anode and cathode of the sensors were connected differentially to the NINO input and also to a transimpedance amplifier to measure energy response (figure 3(a)). The external trigger from the laser, the output of the NINO, and the output of the transimpedance amplifier were digitized by a Lecroy Waverunner 104Xi 1 GHz oscilloscope at 10 GS s^{-1}. Bias of SiPMs and leading edge threshold on the single photon pulses were parametrically varied to find the optimum combination of both. Time delay histograms were fitted with equation (1), which is a convolution of Gaussian and exponential functions. The exponential portion of this equation accounts for delayed signals generated by photons that are converted deeper in the junction of cells comprising the SiPM, which is typically observed in SPTR measurements (Acerbi *et al* 2014a). The SPTR was taken as the raw full-width-at-half-maximum (FWHM) of the fitted curve.

$$f(t;\mu;\sigma;\lambda) = \frac{\lambda}{2} e^{\frac{\lambda}{2}(2\mu+\lambda\sigma^2-2t)} \left[1 - erf\left(\frac{\mu+\lambda\sigma^2-t}{\sqrt{2}\sigma}\right)\right]. \quad (1)$$

The experimental setup to measure SPTR with the compensation circuit is shown in figure 3(b). For these measurements the waveforms from the readout were directly digitized, along with the external trigger of the laser. The laser repetition rate used was 10 kHz. In post-processing, a 10 ns region of the signal baseline just before the rise of the single photon pulses was averaged and used to correct for baseline fluctuations. Leading edge threshold was optimized, and time delay histograms were fitted with equation (1). An example of a time delay histogram for these SPTR measurements with the fitted curve is shown in figure 4. SPTR was taken as the raw FWHM of the

Table 1. List of SiPM samples from various producers and breakdown voltages.

SiPM	Device area (mm^2)	Cell size (μm)	Breakdown voltage (V)
FBK near ultra violet SPAD	0.04 × 0.04	40	26.2 ± 0.1
FBK near ultra violet	1 × 1	40	26.2 ± 0.1
FBK near ultra violet	3 × 3	40	26.2 ± 0.1
FBK near ultra violet high density	4 × 4	40	25.8 ± 0.1
Hamamatsu low cross talk 2	3 × 3	50	47.5 ± 0.1
SensL JD0	3 × 3	35	24.7 ± 0.1

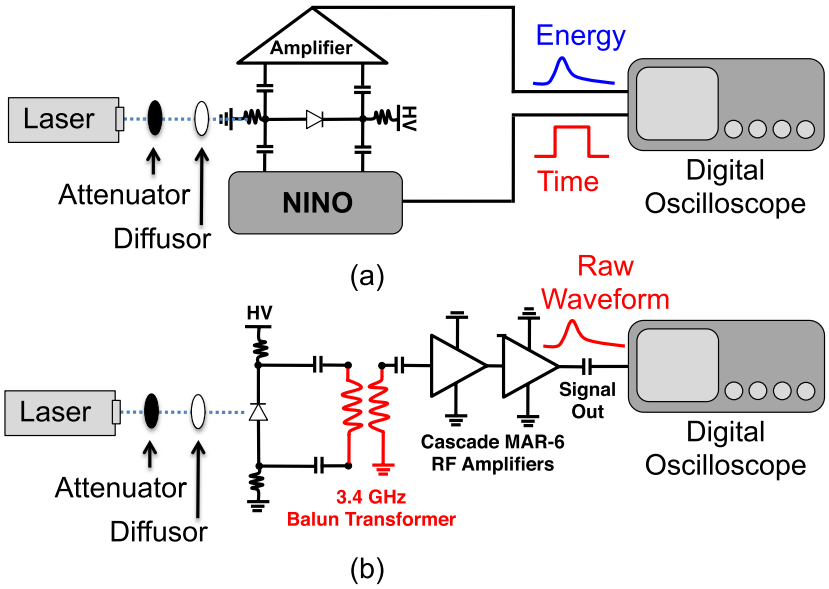

Figure 3. The experimental setup used to measure SPTR with the NINO is shown in (a) (Nemallapudi *et al* 2016), and the setup to test the circuit shown in figure 2(b) is shown in (b).

fitted curve. For each SiPM and overvoltage configuration 20 000 events were analyzed. The statistical error for SPTR at each overvoltage was found by dividing the data into three sets that were analyzed separately to find a mean SPTR with an associated standard deviation.

The contribution of electronic noise on timing performance was also calculated from the digitized waveforms according to the procedure outlined in figure 5. Electronic noise was estimated from a histogram of baseline noise before the single photon pulses, where sigma was extracted from a fit to the resulting distribution. The slope of single photon waveforms was found by averaging all single photon pulses and measuring (dV/dt) for a range of thresholds along the leading edge of the pulse. These data provided inputs for the equation in the bottom right of figure 5, yielding an estimate of the contribution from electronic noise to SPTR.

3. Results

3.1. Electronic noise contribution to timing jitter with the compensation circuit

The calculated electronic noise contribution to timing jitter for voltage sweeps on all the devices when using the compensation circuit is shown in figure 6 (reported in FWHM). For SiPM overvoltage in ranges optimum for coincidence time resolution measurements (>6 V for FBK , >6.5 V for SensL J SiPMs and >4 V for HPK) the calculated electronic noise contribution is ⩽60 ps FWHM for all devices, and the electronic noise contribution at higher bias reached as low as <35 ps FWHM for many of the sensors. The expected electronic noise contributions to timing jitter shown in figure 6 are substantially lower than the SPTRs measured for these devices in Nemallapudi *et al* (2016). Therefore, if the major contribution to SPTR is electronic noise (Acerbi *et al* 2014a, 2015a), these data indicate the compensation circuit provides a readout for testing achievable SPTR when jitter due to electronic noise is minimized.

3.2. SPTR measurements with various analog SiPMs

The measured SPTRs for a FBK NUV 40 μm width single photon avalanche photodiode (SPAD), 1 × 1 mm^2 FBK NUV SiPM, (40 μm cell size), and 3 × 3 mm^2 FBK NUV SiPM (40 μm cell size) are shown as a function of

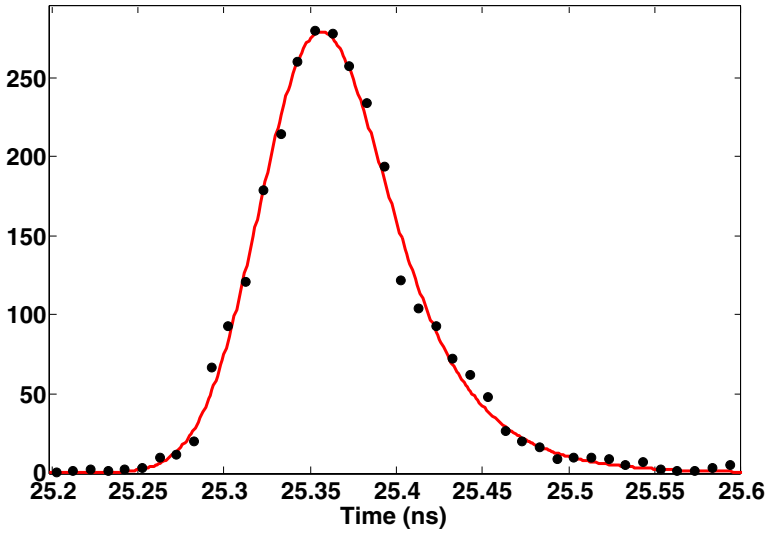

Figure 4. Example of a histogram of delay between external trigger from laser and arrival of single photon pulses. The distribution was fit with equation (1), and SPTR was taken directly from the FWHM of the fit, not from any fit parameters.

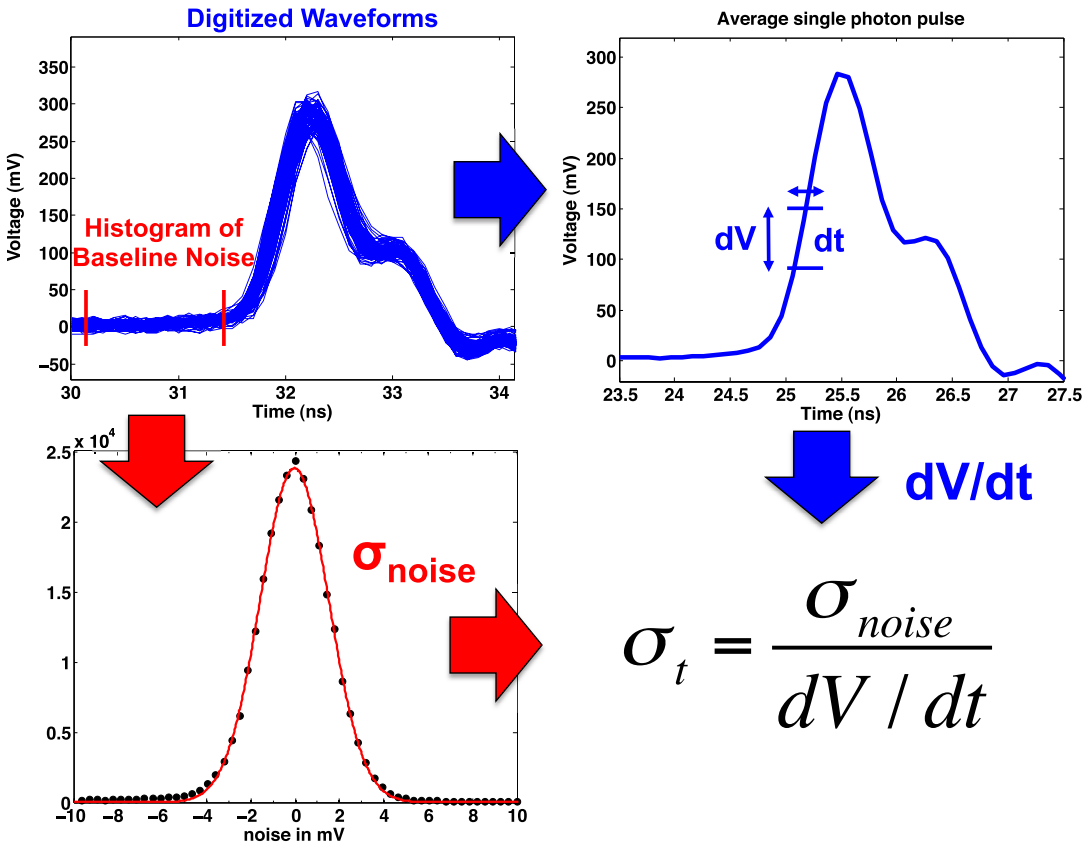

Figure 5. The method used to extract electronic noise and signal slope to calculate the contribution of electronic noise on SPTR is shown.

applied overvoltage in figure 7. For measured SPTR with the single SPAD, both the NINO and the compensation circuit converge to the same value. This behavior is expected, as the contribution of electronic noise to SPTR is not dominant for a single Geiger-mode avalanche photodiode. An amplitude versus time walk correction was also applied to the digitized data to investigate any further improvement SPTR when the effects of amplitude walk on the leading edge time estimate were taken into consideration. An example of the time walk correction applied to the single SPAD when biased at 37 V is shown in figure 8. The minimum value for the 'as measured' and time 'walk corrected' data are also given for each data set in figure 7(a). One unexpected behavior of the single SPAD was slightly higher SPTR than the $1 \times 1\,\text{mm}^2$ SiPM at low overvoltages. The statistical bounds of the

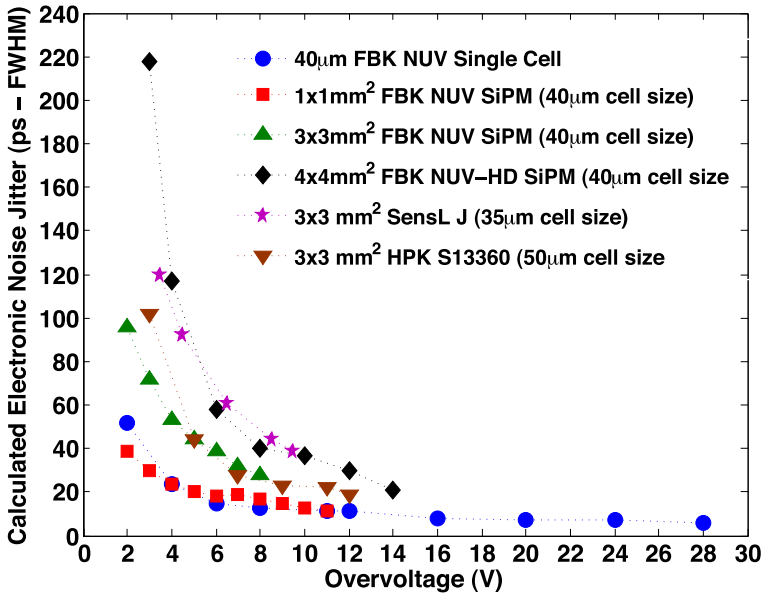

Figure 6. Calculated electronic noise contribution to SPTR for the devices measured in this work (list in table 1) for a sweep of applied bias.

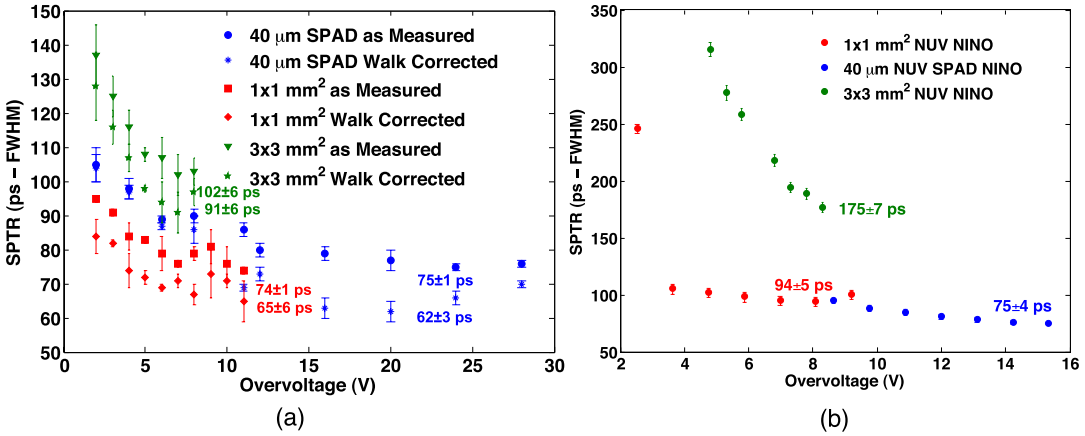

Figure 7. Measured SPTR for a single 40 μm FBK NUV cell, 1 $\times$ 1 mm^2 FBK NUV (also with 40 μm Geiger cell size) SiPM, and 3 $\times$ 3 mm^2 FBK NUV (also with 40 μm Geiger cell size) SiPM is shown with the NINO ASIC (b) and compensation circuit (a).

error on the SPAD and 1 $\times$ 1 mm^2 as-measured SPTRs differ by a small range of 4-to-9 ps at lower applied bias. However, as the voltage applied to the single SPAD was increased above V_{br} + 10 V, the minimum SPTR values matched those reported for the 1 $\times$ 1 mm^2 SiPM. We expand on potential reasons for this behavior at very low overvoltages in section 4.1.

The measured SPTR with a 3 $\times$ 3 mm^2 FBK NUV SiPM is also shown separately in figure 9(a) with the NINO and compensation circuit. For this case, SPTR measured with the NINO was about 75% higher. The measured SPTR with a 4 $\times$ 4 mm^2 FBK NUV-HD SiPM is shown in figure 9(b), where a 26% higher value with the NINO chip was observed. The calculated electronic noise contributions to SPTR for the 3 $\times$ 3 mm^2 FBK NUV SiPM and 4 $\times$ 4 mm^2 NUV-HD SiPM at optimum overvoltage were 33 and 31 ps FWHM, respectively. The expected SPTR if the remaining electronic noise contribution to SPTR was quadratically subtracted from the measured values is represented as a function of overvoltage with a dashed red line in figures 9(a) and (b).

SPTRs for 3 $\times$ 3 mm^2 HPK S13360 (50 μm Geiger cell size) and SensL J (35 μm Geiger cell size) SiPMs are shown in figures 10(a) and (b), respectively. For these sensors, 51% and 92% higher SPTR values were measured with the NINO, compared to the compensation circuit with the HPK and SensL SiPMs, respectively. The calculated electronic noise contribution to SPTR for the HPK and SensL SiPMs at optimum overvoltage were 22 and 47 ps FWHM, respectively. The expected SPTR if the remaining electronic noise contribution to SPTR was also quadratically subtracted from the measured values is represented as a function of overvoltage with a dashed red line in figures 10(a) and (b).

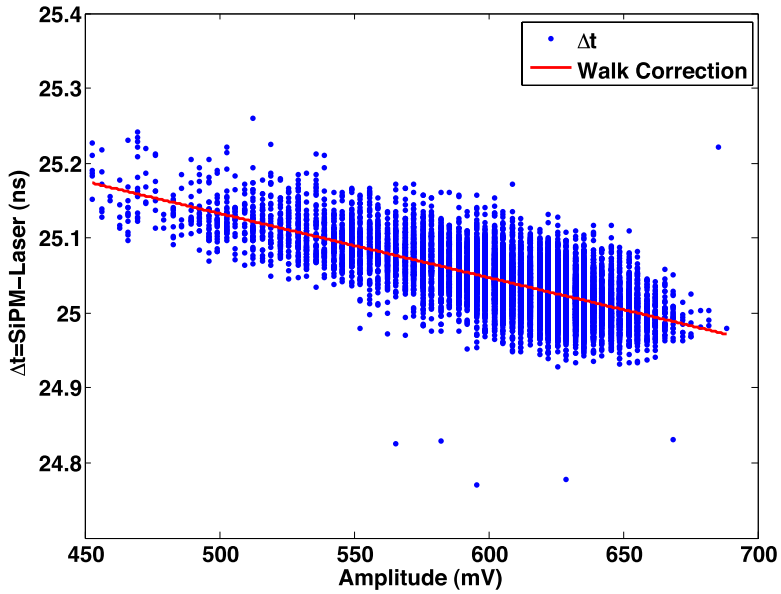

Figure 8. Example of amplitude versus time walk correction applied to the single 40 μm FBK NUV SPAD at a bias of 37 V.

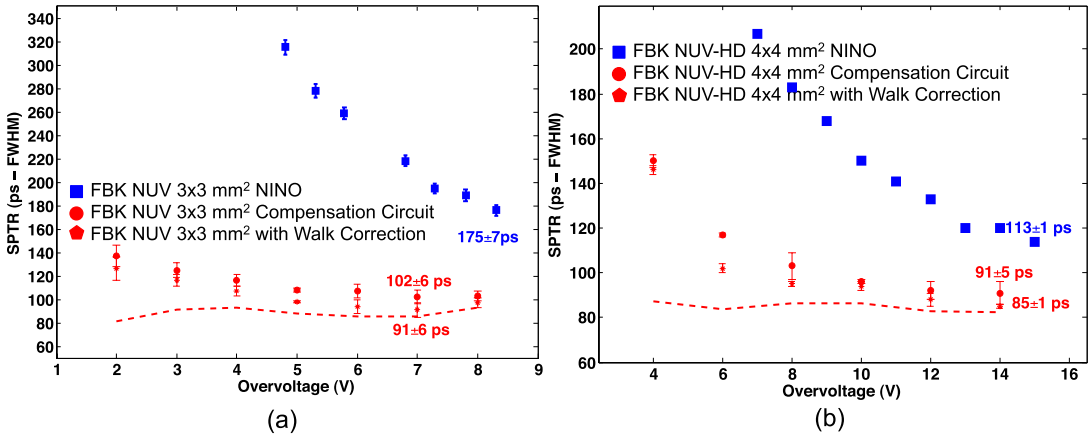

Figure 9. Measured SPTR versus overvoltage for 3 × 3 mm^2 FBK NUV SiPM with 40 μm cell size is shown in (a), and in (b) SPTR is shown for 4 × 4 mm^2 FBK NUV-HD SiPM with 40 μm cell size.

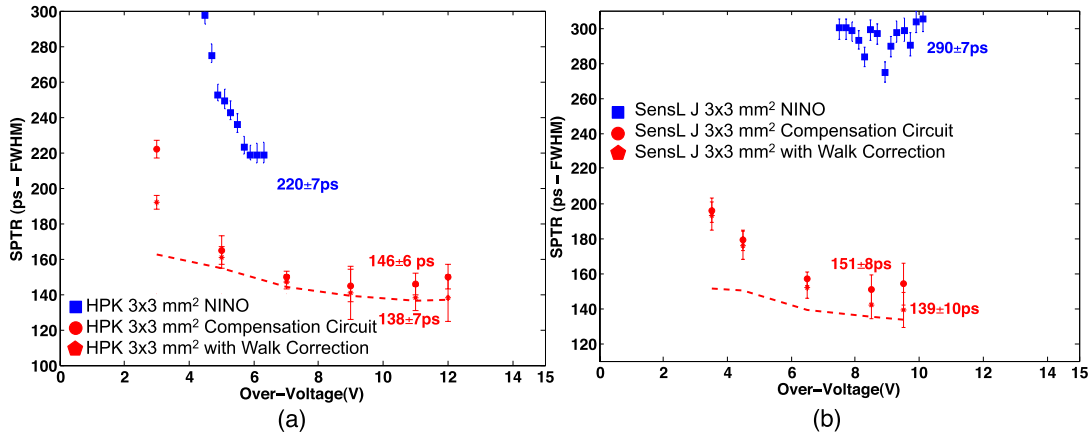

Figure 10. SPTR versus overvoltage for 3 × 3 mm^2 HPK S13360 SiPM is shown in (a), and in (b) SPTR measured with a 3 × 3 mm^2 SensL J SiPM is shown.

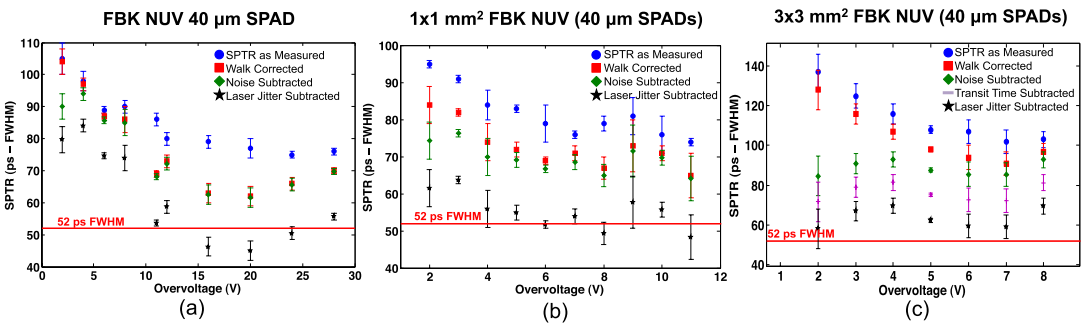

Figure 11. As measured and expected SPTR when various factors that degrade SPTR are taken into account for single 40 μm FBK NUV SPADs (a), a 1 $\times$ 1 mm^2 FBK NUV SiPM also with 40 μm cells (b), and a 3 $\times$ 3 mm^2 FBK NUV SiPM also with 40 μm cells (c).

Having measured SPTR for NUV SiPMs consisting of a single SPAD, as well as 1 $\times$ 1 mm^2 and 3 $\times$ 3 mm^2 areas comprising hundreds to thousands of Geiger cells, allows for some further investigation into improving SPTR. For the large area, 3 $\times$ 3 mm^2 NUV SiPM with 40 μm cell size, even when the electronic noise was minimized, the measured SPTR did not approach that observed for a single SPAD (figure 9(a)). If the contribution from electronic noise could be completely removed, quadratically subtracting the remaining 33 ps electronic noise contribution at 7V overvoltage from the measured 100 ps SPTR provides an expected SPTR of 94 ps. Therefore, other factors must be contributing to the observed SPTR. Further analyses to investigate possible factors degrading SPTR for the larger area sensors, are shown in figures 11(a)–(c) for the FBK NUV 40 μm SPAD, 1 $\times$ 1 mm^2 NUV SiPM with 40 μm cell size, and 3 $\times$ 3 mm^2 NUV SiPM with 40 μm cell size. In these analyses, we again performed a simple amplitude-versus-time walk correction to digitized timestamps and also subtracted the contributions from remaining electronic noise, any charge transit effects (Acerbi *et al* 2015b), and the jitter of the laser used in the experimental setup. A red line in figures 10(a)–(c) indicates the mean expected SPTR when all of these factors are taken into account for the single SPAD (for values where the SPAD's SPTR has 'converged' $>V_{br}+10$V). Interestingly, when these analyses are applied to the 3 $\times$ 3 mm^2 SiPM, the expected SPTR closely approaches that for a single SPAD. We discuss these results in more detail in section 4.

4. Discussion

4.1. Improved SPTR by minimizing the influence of electronic noise

With the compensation circuit employing a transformer at the front end of the SiPM readout, the same minimum SPTR achieved with a single FBK NUV 40 μm SPAD was also achieved for an SiPM with many hundreds of Geiger cells in a FBK NUV 1 $\times$ 1 mm^2 device (figure 7(a)). Although, there was an unexpected behavior of the 40 μm SPAD SPTR being slightly higher than the 1 $\times$ 1 mm^2 SiPM at very low overvoltages. There are a number of potential factors that might influence this unexpected behavior. SPADs of the same design can exhibit differences in performance characteristics and measured SPTR, as was shown in Acerbi *et al* (2014a), where the same SPAD design exhibited differences in SPTR outside experimental error. Considering slightly different performance that can exist from SPAD-to-SPAD, the SPTR for a single SPAD with worse performance could then exhibit higher SPTR than an average of many hundreds in a larger area SiPM (1 $\times$ 1 mm^2 in this case). The unexpected behavior at lower overvoltages could also be due to noise pickup from the larger-area circuit board on which it is assembled, considering the calculated electronic noise influence on SPTR was higher for the SPAD at the lowest bias points and equivalent to the 1 $\times$ 1 mm^2 SiPM at higher overvoltages (figure 6).

The observed convergence of the 40 μ SPAD to the same SPTR value as the 1 $\times$ 1 mm^2 SiPM is in line with predictions made by previous work at FBK (Acerbi *et al* 2014a, 2015a). However, the same trend did not continue with increasing device area. While the compensation circuit did improve the SPTR for FBK NUV SiPM of 3 $\times$ 3 mm^2 area from 175 to 100 ps (figure 9(a)), SPTR did not converge to the 75 ps value measured for a single SPAD. Therefore, there are other contributing factors. One possibility is differences in trace lengths, and hence stray capacitance and inductance for different cells. Different trace lengths cause different impedances that can result in a variation in single photon amplitude and shape. This variation in single photon amplitude creates an amplitude walk. The amplitude versus time walk correction applied in figures 8–10 should compensate for this, but still the walk-corrected SPTRs for the large area FBK SiPMs did not reach the minimum value measured for the single 40 μm SPAD. Therefore, when the influence of electronic noise is minimized and effects that induce additional jitter from amplitude walk are compensated for, other factors (ex. charge transit time skew) are likely no longer negligible for these large area SiPMs. Ultimately, SPTR of both single SPADs and large area devices is limited by a position of interaction dependence within a single cell of an SiPM due to edge effects that arise from

non-uniformities in the electric field at the walls of the SPADs (Nemallapudi *et al* 2016, Lecoq 2017). We further discuss limitations on SPTR in the next section.

SPTR was also improved for 3×3 mm^2 HPK and SensL SiPMs with the compensation circuit (figures 10(a) and (b)), but SPTR below 100 ps FWHM was not achieved in these measurements. For the HPK SiPM tested, this might be due to a relatively larger portion of the cell being susceptible to the edge effects discussed in Nemallapudi *et al* (2016) and Lecoq (2017). Since a significant portion of the cells comprising the HPK SiPM is susceptible to these edge effects that degrade SPTR, this can also result in an overall higher SPTR for a large area device. For the SensL SiPM, to make a direct comparison to the measurements made with the NINO ASIC, the standard terminal was used to measure SPTR, where signal must pass through the quenching resistor of the SiPM. The fast, AC-coupled component of the single photon waveform is isolated to a separate fast terminal. If the measurement was repeated with the fast terminal, the fast component of the single photon response could potentially provide an improved SPTR. Future work will investigate the achievable SPTR with waveforms from the fast terminal and also the influence of edge effects on Geiger cells of SensL SiPMs.

4.2. Potential to further improve SPTR for large area analog SiPMs

The different factors affecting achievable SPTR can be broken down into the following:

1. Intrinsic SPTR for a single cell affected by the electric-field non-uniformity across the cell and temporal kinetics of the avalanche within it.
2. The effect that electronic noise has on SPTR
   (a) Degraded single photon response shape and SNR with increasing device area due to an equally increasing parasitic capacitance.
   (b) Electronic noise and bandwidth of the front-end readout electronics of the SiPM. (Preamplifiers, amplifiers, etc.)
3. Variations in trace length from individual cells to readout nodes of the devices.
   (a) Charge transit time skew variations.
   (b) Variations in impedance due to different trace lengths that can result in variations of single photon pulse shape/amplitude, creating increased jitter due to an amplitude-walk.

Factors described in item 1 will inherently limit the ultimate achievable SPTR, and these must be addressed on a very fundamental level in the device design. Lower SPTR values than those presented here have been achieved for single SPADs with smaller diameter or by covering the edge area of the SPAD with a metalized light shielding to circumvent the edge effect on SPTR. For those cases, SPTR on the order of ~20 ps FWHM has been achieved (Acerbi *et al* 2014b).

In this work, we specifically focused on addressing item 2, as earlier work had predicted this to be a major contributor to degraded SPTR when not addressed properly. Indeed, when the contribution of electronic noise was minimized, substantial improvements in SPTR were observed. When the effects of electronic noise are minimized (as in this work), factors addressed in items 3(a) and 3(b) are likely no longer negligible for large area SiPMs. The influence of variations in trace length has been explored in previous works for FBK SiPMs, with regards to charge transit time skew (Acerbi *et al* 2015b). A maximum variation in charge transit time of ~45 ps was observed across 3×3 mm^2 SiPMs with a three-terminal readout of signal from the cells, as was the case for the 3×3 mm^2 NUV SiPM used in this work.

As a last point, we consider the estimated SPTR for the FBK NUV devices (single 40 μm SPAD, 1×1 mm^2 and 3×3 mm^2 SiPMs also with 40 μm cell size) when effects described in items 1–3 are minimized or removed. This is shown in figures 11(a)–(c). Again, a simple pulse amplitude-versus-time walk correction was applied to the timestamps from the digitized waveforms acquired from each device. This time walk correction is a method to minimize or correct for the influence trace impedance variations on single photon pulse shape (item 3(b)). The remaining calculated influence of electronic noise on SPTR (item 2) was then quadratically subtracted. The contribution to transit time skew in the 3×3 mm^2 sensor (Acerbi *et al* 2015b) (item 3(a)) and the jitter of the laser were then subsequently subtracted. A similar estimated SPTR is obtained for the three sensor sizes when all these factors described in items 1–3 are taken into consideration. Note, no transit time skew is removed from the single cell or 1×1 mm^2 SiPM, as it was found in Acerbi *et al* (2015b) that the transit time skew of 1×1 mm^2 devices was negligible. This result was also observed in the measurements presented in figure 8, where the same SPTR for a single SPAD and 1×1 mm^2 FBK NUV SiPM was obtained, which is in agreement with this assertion. The analyses in figures 11(a)–(c) indicate that if improvements can be made on variations in trace length/impedance, the SPTR for large area analog SiPMs could potentially be further improved toward that measured for a single cell.

5. Conclusions and outlook

Front-end electronics that minimize the influence of electronic noise can make substantial improvements on SPTR for large area, analog SiPMs. In this work, we tested a circuit with the potential to reduce the contribution of electronic noise on SPTR through improvements in single photon pulse shape, via a reduced effective device capacitance. With this readout, the same SPTR achieved for a single 40 μm FBK NUV cell was also achieved with a $1 \times 1\,\mathrm{mm}^2$ FBK NUV SiPM with the same cell size. The compensation circuit also significantly reduced measured SPTR for larger area SiPMs, resulting in $\leqslant$100 ps FWHM SPTR for FBK devices 3×3 mm^2 and 4×4 mm^2 in area and $\leqslant$150 ps FWHM for 3×3 mm^2 HPK and SensL SiPMs. This readout technique is a promising solution to improve SPTR with large area analog SiPMs, which could potentially open avenues to improve CTR for TOF-PET detectors that exploit a small number of prompt photons to derive a precise estimate for 511 keV photon time of interaction.

Acknowledgments

This work was supported in part by the Stanford Molecular Imaging Scholars Program (SMIS) (NIH-NCI 2T32 CA118681-11A1) and R01 CA214669. This work was also carried out in frame of Crystal Clear Collaboration and Cost Action TD1401 (FAST) and supported in part by one of the author's ERC Advanced Grant TICAL #338953 and the related Proof-of-Concept project ULTIMA #680552, both funded by the European Commission.

References

Acerbi F, Ferri A, Gola A, Cazzanelli M, Lorenzo P, Zorzi N and Piemonte C 2014a Characterization of single-photon time resolution: from single SPAD to silicon photomultiplier *IEEE Trans. Nucl. Sci.* **61** 2678–86

Acerbi F, Cazzanelli M, Ferri A, Gola A, Pavesi L, Zorzi N and Piemonte C 2014b High detection efficiency and time resolution integrated-passive-quenched single-photon avalanche photodiodes *IEEE J. Sel. Top. Quantum Electron.* **20** 3804608

Acerbi F, Ferri A, Gola A, Zorzi N and Piemonte C 2015a Analysis of single photon time resolution of FBK silicon photomultipliers *Nucl. Instrum. Methods* A **787** 34–47

Acerbi F, Gola A, Ferri A, Zorzi N, Paternoster G and Piemonte C 2015b Analysis of transit time spread on FBK silicon photomultipliers *J. Instrum.* **10** P07014

Brunner S E and Schaart D R 2017 BGO as a hybrid scintillator/Cherenkov radiator for cost-effective time-of-flight PET *Phys. Med. Biol.* **62** 4421–39

Cates J W and Levin C S 2016 Advances in coincidence time resolution for PET *Phys. Med. Biol.* **61** 2255–65

Cates J W, Vinke R and Levin C S 2015 Analytical calculation of the lower bound on timing resolution for PET scintillation detectors comprised of high-aspect-ratio crystal elements *Phys. Med. Biol.* **60** 5141–61

Gola A, Piemonte C and Tarolli A 2011 Analog circuit for timing measurements with large area SiPMs coupled to LYSO crystals *IEEE NSS MIC Conf. Record* pp 725–31

Gola A, Piemonte C and Tarolli A 2012 The DLED algorithm for timing measurements on large area SiPMs coupled to scintillators *IEEE Trans. Nucl. Sci.* **59** 358–65

Gundacker S, Acerbi F, Auffray E, Ferri A, Gola A, Nemallapudi M V, Paternoster G, Piemonte C and Lecoq P 2016a State of the art timing in TOF-PET detectors with LuAG, GAGG, and L(Y)SO scintillatorsof various sizes coupled to FBK-SiPMs *J. Instrum.* **11** P08008

Gundacker S, Auffray E, Frisch B, Jarron P, Knaptisch A, Meyer T, Pizzichemi M and Lecoq P 2013 Time of flight positron emission tomography towards 100 ps resolution with L(Y)SO: an experimental and theoretical analysis *J. Instrum.* **8** P07014

Gundacker S, Auffray E, Pauwels K and Lecoq P 2016b Measurement of intrinsic rise times for various L(Y)SO and LuAG scintillators with a general study of prompt photons to achieve 10 ps in TOF-PET *Phys. Med. Biol.* **61** 2802–37

Kwon S I, Gola A, Ferri A, Piemonte C and Cherry S R 2016a Bismuth germinate coupled to near ultraviolet silicon photomultipliers for time-of-flight PET *Phys. Med. Biol.* **61** 38–47

Kwon I, Kang T and Hammig M K 2016b Experimental validation of charge-sensitive amplifier configuration that compensates for detector capacitance *IEEE Trans. Nucl. Sci.* **63** 1202–8

Kwon I, Kang T, Wells B T, D'Aries L J and Hammig M D 2015 Compensation of the detector capacitance presented to charge-sensitive preamplifiers using the Miller effect *Nucl. Instrum. Methods* A **784** 220–5

Lecoq P 2017 Pushing the limits in time-of-flight PET imaging *IEEE Trans. Radiat. Plasma Sci.* **1** 473–85

Lecoq P, Korzhik M and Vasiliev A 2014 Can transient phenomena help improving time resolution in scintillators *IEEE Trans. Nucl. Sci.* **61** 229–34

Levin C S and Hoffman E J 1999 Calculation of positron range and its effect on the fundamental limit of positron emission tomography system spatial resolution *Phys. Med. Biol.* **45** 559

MACOM 2018 MABA-007159 data sheet www.cdn.macom.com/datasheets/MABA-007159-000000.pdf

Minicircuits 2017 MAR-6 RF amplifier data sheet www.minicircuits.com/pdfs/MAR-6+.pdf

Nemallapudi M V, Gundacker S, Lecoq P and Auffray E 2016 Single photon time resolution of state of the art SiPMs *J. Instrum.* **11** P10016

Nemallapudi M V, Gundacker S, Lecoq P, Auffray E, Ferri A, Gola A and Piemonte C 2015 Sub-100 ps coincidence time resolution for positron emission tomography with LSO:Ce codoped with Ca *Phys. Med. Biol.* **60** 4635–49

Otte A N, Garcia D, Nguyen T and Purushotham D 2017 Characterization of three high efficiency and blue sensitive silicon photomultipliers *Nucl. Instrum. Methods* A **846** 106–25

Piemonte C, Acerbi F, Ferri A, Gola A, Paternoster G, Regazzoni V, Zappala G and Zorzi N 2016 Performance of NUV-HD silicon photomultiplier technology *IEEE Trans. Electron Devices* **63** 1111–6

SensL 2017 J series SiPM datasheet www.sensl.com/downloads/ds/UM-MicroJ.pdf
Schaart D R, Seifert S, Vinke R, van Dam H T, Dendooven P, Lohner H and Beekman F J 2010 LaBr3:Ce and SiPMs for time-of-flight PET: achieving 100 ps coincidence resolving time *Phys. Med. Biol.* **55** N179–89
Seifert S, van Dam H T and Schaart D R 2012 The lower bound on the timing resolution of scintillation detectors *Phys. Med. Biol.* **57** 1797–814
Seifert S, Vinke R, van Dam H T, Lohner H, Dendooven P, Beekman F J and Schaart D R 2009 Ultra precise timing with SiPM-based TOF PET scintillation detectors *NSS/MIC: IEEE Nuclear Science Symp. Conf. Record (Orlando)* pp 2329–33
Zhang N and Schmand M J 2016 Bootstrapping readout for large terminal capacitance analog-SiPM based time-of-flight PET detector *US Patent* US2016/0327657